Combined EXAFS and *ab initio* study of copper complex geometries adsorbed on natural illite

David M. S. Martins,[†,‡] José P. Mirão,[§] Joerg Goettlicher,[¥] Marco Molinari,[‡,⊥] Ralph Steininger,[¥] Stephen C. Parker [‡] and Mário A. Gonçalves[†,*]

[†] Departamento de Geologia and Instituto Dom Luiz, Faculdade de Ciências, Universidade de Lisboa, 1749-016 Lisboa, Portugal

[‡] Department of Chemistry, University of Bath, Claverton Down, Bath, BA2 7AY, United Kingdom

[⊥] Department of Chemistry, University of Huddersfield, Huddersfield HD1 3DH, United Kingdom

[§] Geoscience Department and HERCULES, University of Évora, Apt. 94, 7002-554 Évora, Portugal.

[¥] Karlsruhe Inst. of Technol., ANKA Synchrotron Radiat. Facil., D-76344 Eggenstein Leopoldshafen, Germany

*Corresponding author at: Departamento de Geologia, Faculdade de Ciências, Universidade de Lisboa, Edifício C6, Piso 4, Campo Grande, 1749-016 Lisboa, Portugal. Tel.:+351 217500361; Fax: +351 217500064.

E-mail: mgoncalves@ciencias.ulisboa.pt

ABSTRACT

The adsorption of copper on the 2:1 clay mineral illite (0.4 to 20 μm in size) was studied using a combination of extended X-ray adsorption fine structure (EXAFS) and hybrid-Density Functional Theory (DFT) modelling. The study evaluates the effect of varying pH and copper concentration on the mechanisms of copper adsorption in solutions at background electrolyte concentration typical of natural surface continental freshwaters in granitic environments. The EXAFS spectra revealed both the elongated square pyramidal and Jahn-Teller octahedral coordinated copper clusters as feasible with the former providing better fits using spertiniite (crystalline copper hydroxide) as model compound. Additionally, *ab initio* calculations also predicted the square pyramidal geometry to be more stable. Copper ions have four O_{eq} at an average distance of 1.95(1) Å and two independent O_{ax} at average distances of 2.32(16) Å and 3.06(9) Å, with the latter decreasing to 2.97(2) Å as copper concentration and pH are increased. This may reveal different mechanism by which copper adsorbs on illite, as a weakly bound complex at low pH likely at exchange and edge sites and changing towards more strongly bound complexes at high affinity edge sites at higher pH and copper loads. Above 1% Cu model fits suggest formation of copper oligomers with average Cu-Cu distance of 3.10(2) Å. These occur at pH greater than 6, where the correlation between Cu-Cu and Al-Al distances in the illite edge surfaces supports the formation of surface precipitates.

Keywords: Clay minerals, illite, copper adsorption, edge surfaces, Cu K-edge EXAFS, *ab initio* calculations.

1. INTRODUCTION

An understanding of the interaction of metal ions with mineral surfaces is a key requirement for assessing the fate of metals in the environment (Bradl, 2004; Egirani *et al.*, 2005; Mellouk *et al.*, 2011). Clay minerals are among the most important inorganic phases in natural systems due to their high exchange and adsorption capacities of metal ions, and they have been considered in many applications including remediation of mining areas and radioactive waste disposal facilities, as well as engineered retention and reactive barriers (Sanchez *et al.*, 1999; Vengris *et al.*, 2001; Alvarez-Puebla et al., 2005; Uddin, 2017). Thus developing models for the mechanisms of retention of metal ions on clays is fundamental to predicting their fate and obtaining an accurate evaluation of the environmental risks.

Surface complexation modelling (SCM) is a well-established approach to evaluate the condition of metal retention and stability at the mineral-water interface (Sherman, 2009). While SCM has proven successful in providing insight for the molecular scale mechanisms, additional structural information (coordination geometries) of the adsorbed metals onto surfaces is needed to validate the models. Structural insights are generally achieved using X-ray Absorption Spectroscopy (XAS) performed at synchrotron radiation sources (Cheah *et al.*, 1998; Scheidegger *et al.*, 1998; Thompson *et al.*, 2000; Brigatti *et al.*, 2004; Peacock and Sherman, 2004, 2005a; Peacock and Sherman, 2005b; Schlegel and Manceau, 2013) or more recently using atomistic modelling (Kerisit and Parker, 2004; Martins *et al.*, 2009; Martins *et al.*, 2014; Zhang et al., 2016; Zhang et al., 2017).

Amongst the transition metals, copper is a common cation, and its environmental concentration has increased due to a diversity of anthropogenic activities, such as

mining, manufacturing, agriculture, and waste disposal (Berti and Jacobs, 1996; Madrid and Díaz-Barrientos, 1998). Adsorption studies of copper onto clay minerals have been generally focused on swelling clays, especially montmorillonite (Papelis and Hayes, 1996; Scheidegger *et al.*, 1998; Chen and Hayes, 1999; Hyun *et al.*, 2000; Morton *et al.*, 2001; Dähn *et al.*, 2003; Brigatti *et al.*, 2004; Schlegel and Manceau, 2006; Yang er al., 2015), whereas less attention has been paid to the role of non-swelling clays (Hesterberg *et al.*, 1997; Chen and Hayes, 1999; Gier and Johns, 2000; Flogeac *et al.*, 2004; Alvarez-Puebla et al., 2005; Sajidu et al., 2008; Strawn and Baker, 2009; Bradbury and Baeyens, 2009; Turan et al., 2011). However, non-swelling clays, such as illite, are amongst the most common phyllosilicates at the Earth surface (Srodon and Eberl, 1984; Du *et al.*, 1997) and can be de dominant clay mineral in some surface environments, such as in poorly developed soils in granitic areas (Gonçalves et al., 2004). Therefore, their interaction with metals such as copper and many others may significantly control their distribution and partitioning between the terrestrial and aqueous environment. Many factors control the adsorption of transition metals onto clay minerals, such as, the structure of the adsorbate metal species, surface composition, and charge which in turn largely depend on the aqueous environment conditions in contact with the mineral phase. However, some of these factors have not been fully addressed yet, and lack of a general theoretical basis that can predict unequivocally how and where does a transition metal ion adsorbs on a mineral surface still requires the exploration of particular systems under pre-determined aqueous solution conditions. For example, the structure (coordination and geometry) of the adsorbed copper cluster onto clay minerals has been subject of debate, with 6-, 5- and 4-fold coordination clusters and possibly even dynamic coexistence having all been proposed (*e.g.*, Bryantsev *et al*., 2008; Frank *et al*., 2015; Hyun and Hayes, 2015; La Penna *et al*., 2015; Liu *et al*., 2015). In contrast,

controlled laboratory experiments normally focus on the influence that variables such as the pH or the background electrolyte concentration have on the adsorption of metals. The choice of adequate conditions defines the type of sites it is possible to probe, either high or low energy sites and cation exchange (Tournassant et al., 2013). However, depending on the substrate geology, many natural surface waters have fairly low electrolyte concentrations ($< 10^{-3}$ M), while heavily polluted circumscribed areas are likely to develop highly concentrated solutions (Gonçalves *et al.*, 2004; Figueiras *et al.*, 2009). In contrast, although several experiments in the literature span a wide range of ionic strength conditions (Tournassant et al., 2013) the majority favor the use of high background electrolyte concentration (≈ 0.1 M) which only in very particular circumstances occur in natural environments. There are also several models for illite surface properties and divalent cation adsorption published in the literature (e.g. Du et al., 1997a; Du et al., 1997b; Alavrez-Puebla et al., 2005; Bradbury and Baeyens, 2009), that do not fully agree. Besides, only a few of the available studies have considered adsorption of copper onto the basal (001) surfaces of montmorillonite, a mechanism that was found to increase as ionic strength decreases (Morton *et al.*, 2001). This situation still raises many uncertainties on the detailed mechanisms and geometrical configurations of divalent metal ions adsorbed onto clay mineral surfaces under typical natural freshwater ionic strength conditions.

In this study, we have used a combined approach of experimental (EXAFS) and modelling techniques (*ab initio* calculations) to study the effect of pH and Cu concentration on the adsorption geometries of copper on pure illite samples to unravel the mechanisms and influence of the non-swelling components of the clay mineral phase on copper adsorption at low ionic strength conditions.

2. METHODOLOGY

2.1. EXAFS sample preparation.

Samples for analysis with EXAFS, were prepared from a series of adsorption experiments performed in batch mode using the IMt-1 illite from Silver Hill, Montana (Cambrian Shale) (Hower and Mowatt, 1966) purchased from the Clay Minerals Society repository of "special clays". To eliminate any surface interfering phase, illite was pre-treated using standard procedures and its physical and chemical characterization was done by SEM-EDS, XRD, and ATR-FTIR at all stages of illite preparation (details in the Supporting Information file for these and other measured parameters of the illite used in this study). Solution pH was chosen according to 3 different groups of aqueous solutions studied and analysed in granitic areas (Figueiras *et al.*, 2009): *i*) pH 4.5, infiltrating shallow groundwater after interaction with organic acids in soils; *ii*) pH 5.5, surface runoff waters in equilibrium with atmospheric CO_2; and *iii*) pH 6.5, solutions showing initial signs of pollution from landfill leachates. The concentration of copper used in the set of experiments ranged between 5×10^{-5} M and 10^{-3} M of $Cu(NO_3)_2$ such that a low, intermediate and high (saturation) concentration of adsorbed Cu on illite are obtained for each experimental set to analyze their differences by EXAFS, using a background electrolyte concentration of 10^{-3} M of KNO_3. The choice of the background electrolyte concentration was based in the average solution conductivities measured in granitic areas which corresponded to salt concentrations varying between slightly higher than 10^{-4} M up to 10^{-3} M. The reactors were filled with 0.20(0) g of illite for 50 mL of solution with the pH adjusted to the previously chosen values. Experiments ran in two stages: **1.** ***Illite pre-conditioning stage***: Illite is suspended in 50 mL of a KNO_3 solution only (10^{-3} M) and the pH is adjusted to 4.5, 5.5, or 6.5. Reactors are sealed and put into an orbital shaker for 24 h. After that time, the suspension is transferred into tubes and

centrifuged at 4000 rpm for 45 minutes. The supernatant is transferred into a glass vial and the pH measured. **2.** ***Adsorption stage***: Another aliquot with 50 mL of a combined $KNO_3/Cu(NO_3)_2$ solution with the same background electrolyte concentration and initial pH but with different copper concentration is added into each centrifuge tube with the illite from the previous step. After vigorous shaking, the content is transferred into the reactors in the orbital shaker. The suspensions are agitated for 24 h and the pH corrected after 12 h with HNO_3, as deemed necessary to restore the initial pH of the solution. After the 24 h agitation, the suspensions are centrifuged at 4000 rpm for 45 minutes.

About 2/3 of the supernatant solution is retrieved for pH measurement and copper analysis by atomic absorption spectroscopy (Varian SPECTRAA FS 220). The concentration of copper adsorbed onto illite is determined by the difference between the initial and final solution copper concentration normalized to the mass of adsorbent used in each experiment. The remaining portion is transferred into a crucible for filtration under vacuum using 0.20 μm membranes. A small volume of distilled water is added to wash the excess copper solution in the illite paste which is retrieved for the X-ray absorption fine structure (EXAFS) measurements.

2.2. EXAFS experiments.

The EXAFS Cu-K edge measurements were conducted in the Laboratory for Environmental Studies (SUL-X) of the ANKA synchrotron facility (KIT, Germany). The light beam is produced in a Wiggler radiation source, monochromated with Si(111) crystals in a double-crystal monochromator and focused to approximately 50 × 50 μm by an elliptical Kirkpatrick-Baez mirror system. The intensity of the incident beam (I_o) was measured using the first ionisation chamber. The energy calibration was achieved measuring repeatedly a Cu-foil as reference (8.979 keV, first inflection point).

Spertiniite ($Cu(OH)_2$) and tenorite (CuO) were used as model materials, with the crystals structures obtained from Oswald et al. (1990) and Calos et al. (1996), respectively. The fine powdered copper models were measured as pressed pellets in transmission mode. When necessary they were finely ground and homogeneously dispersed in cellulose pellets.

The samples were mounted between two Kapton films and measured in fluorescence mode. The Cu Kα X-ray fluorescence emission radiation was collected using an energy dispersive 7 element Si(Li) fluorescence solid state detector (SGX Sensortech, former Gresham). A 45° geometry was used between the incident radiation beam and the sample and a 90° geometry between the incident beam and the detector. The experimental absorption coefficient (μ), for a given element, was obtained by taking the ratio of the fluorescence detector signal to the signal of the incident photon beam from the first ionization chamber (I_f/I_o).

The data was evaluated using the ATHENA and ARTEMIS codes from IFEFFIT package programs in the graphical interface DEMETER (Ravel and Newville, 2005). Multiple scans were normalized relative to E_o (determined from the inflection point of the derivative of the spectra) and merged. The baseline correction was performed. Subsequently, the spectra were changed from energy dependence to photoelectron wave number (k). The EXAFS signal χ(k) was extracted from experimental data, and Fourier transformed for the data range from k = 3.4 to 11.8 $Å^{-1}$ using a Kaiser-Bessel window. The theoretical amplitudes and phases for the chosen scattering paths were calculated using FEFF8.2 (Ankudinov *et al.*, 1998) taking the reference materials as model structures for Cu-O and Cu-Cu pairs.

Prior to fitting, EXAFS data were Fourier filtered over R-range 1-3 Å, using a Hanning window. A common procedure during the beginning of the fitting process is to rely on

the use of restraints to ensure the physicality of the parameters obtained, even though in the majority of the cases they were not necessary during the fitting of the data. The current work was mainly based on default weights with the different ranges as follows: i) O_{ax} had $0.5<S_0^2<1.1$ and $-0.05<\Delta R<0.05$; ii) O_{eq} had $0.5<S_0^2<1.1$, $-0.5<\Delta R<0.5$ and $0.001<\sigma^2<0.010$; iii) copper oligomers had $0.5<S_0^2<1.2$, $-0.5<\Delta R<0.5$ and $0.001<\sigma^2<0.015$.

2.3. *ab initio* calculations.

Electronic calculations were conducted using the Gaussian03 package (Frisch *et al.*, 2003). Full structural optimizations were carried out using hybrid DFT functional B3LYP (Lee *et al.*, 1988; Becke, 1993), coupled to 6-311G(d,p) basis set (Krishnan *et al.*, 1980; McLean and Chandler, 1980; Frisch *et al.*, 1984) for each of the copper configurations. These calculations were performed for the $Cu(H_2O)_6$, $Cu(H_2O)_5$ and $Cu(OH)_2(H_2O)_4$ configurations in the gas-phase (g) and aqueous system (l), the latter resorting to the polarized continuum model using the integral equation formalism (Cances *et al.*, 1997; Mennucci *et al.*, 1997; Mennucci and Tomasi, 1997; Tomasi *et al.*, 1999). Vibrational frequency calculations were subsequently carried out on all optimized structures to ensure that energy minima had been reached.

3. RESULTS

3.1. Batch experiments.

Adsorption of Cu onto illite suspensions is presented as adsorption isotherms (Fig. 1 with fitted models, and Fig. S4 in SI file with a combined plot of the raw data only). Bulk copper concentrations (adsorbed on illite) ranged between 0.1 and 0.8 wt% illite for the experiments at pH 4.5 and 5.5, while for pH 6.5 copper concentration attained 2.8 wt% illite (weight percentage of copper to mass of adsorbent, herein designated as

mass percentage of copper adsorbed or simply % Cu). The results of batch adsorption experiments show that at both pH 4.5 and 5.5, the adsorption of copper onto illite generally follows a Langmuir-type isotherm, with a steep linear increase for low copper concentration in solution followed by a flattening of the isotherm indicating an approximately constant adsorbed copper concentration as its concentration in solution increases. The experiments at pH 5.5 show higher saturation levels of copper on the surface, with a bulk average concentration around 8 mg Cu/g of adsorbent compared to approximately 4 mg Cu/g of adsorbent for pH 4.5. However, experiments at pH 6.5 show a completely different pattern because as copper in solution is increased so is the copper adsorbed by the illite, never reaching a plateau as in the previous experiments. The relation is nearly linear meaning that copper is continuously withdrawn from solution as the solution gets more and more concentrated, suggesting that a Cu phase may be precipitating on the surface as will be argued later.

3.2 Surface speciation modelling

Previous work has determined the acid-base surface properties of the IMt-1 illites (Gonçalves, 2006) to be in general agreement with the properties determined by Du et al. (1997a). The model was further refined for the number of sites and retaining 1 pK_a surface constant (unpublished data) equivalently to one of the models in Du et al. (1997a). Solution and surface speciation was performed with PHREEQC (Parkhust and Appelo, 1999) in equilibrium with atmospheric CO_2 (Fig. S8 in SI) and shows that the hydrated Cu^{2+} dominates in solution at the pH range conditions of the reacted illites for EXAFS analysis. Surafce speciation reactions were taken form Du et al. (1997b) and these indicate that the surface species $\equiv SOCu^{+}$ starts to form at pH > 4 and at pH > 6 $\equiv SOCu_2(OH)_2$ becomes the dominant surface species/precipitate (Fig. S9). Model description and parameters are reported in the SI file.

Using these same model parameters, the isotherms were also successfully modelled with the surface speciation model of Du et al. (1997b), with the exception of the experiments at pH 6.5 (Fig. 1). At pH 4.5 and 5.5, the Diffuse Double Layer (DDL) model was used in agreement with the optimization procedure for estimation of the surface acidity constants, which provided overall good results. However, pH 6.5 required using the CD-MUSIC surface complexation model (Hiemstra and Van Reimsdijk, 1996) implemented in PHREEQC to closely fit the experimental data. It should be noted that the surface precipitate in the model of Du et al. (1997b) was modeled as a solid phase, not as a surface species. This same approach was used for the solution and surface speciation model in Figure S9 (SI) providing a major difference in the amount of Cu withdrawn from the aqueous solution. In Fig. 1 the experimental points with the best SCM results based in the data of Du et al. (1997a; 1997b) and Gonçalves (2006), are plotted along with the surface acid-base constants of Bradbury and Baeyens (1999) for comparison. The results using the adsorption model of Cu on iliite of Alvarez.-Puebla et al. (2005) are provided in the SI file (Fig, S10 and S11).

3.3. EXAFS experiments

3.3.1. Evaluation of the spectra

The Fourier Transform (FT) and the associated inverse Fourier-filtered scattering curve (FT^{-1}) generated from the Cu K-edge EXAFS spectra of copper adsorbed illites are reported in Fig. 2 (see Fig. S7 for the k-space spectra).

The overall changes derived from the variation of pH make a quantifiable impact on the raw spectra and will be detailed independently below (see Fig. 3 for stacked spectra and Fig. S5 for overlapping spectra). At pH 4.5 the increase of copper concentration leads to an increase of feature **IV.** At pH 5.5 the increase of copper concentration shows a decreasing trend of feature **III** but also the increase of features **IV** and **V** as shown in

Fig. 3 b. At pH 6.5 feature **III** decreases even further and virtually disappear at adsorbed copper concentrations above circa 0.6% Cu as can be seen in Fig. 3 c. Furthermore, above 0.6% Cu the features **IV** and **V** show a pronounced increase. Considering the spectra of spertiniite, it can be observed that feature **III** results from combined signal from the first shell oxygens and the most distant axial oxygen, while feature **IV** is the signal of the first Cu shell. On the other hand, the first Cu shell for tenorite is shifted towards feature **III** and partially overlaps the signal from the axial oxygens, which in turn only have a slight contribution to feature **II**.

3.3.2. Spectral analysis

Spectral and model fitting used the model compounds tenorite (CuO), spertiniite ($Cu(OH)_2$) and variants with a mixing character of both. In general, there is a good match in the peak positions and peak intensities when using the experimental spectra of both model compounds, as shown in Fig. 2 for spertiniite and tenorite. The major difference between these model compounds is the coordination environment of copper with respect to the axial oxygen atoms. While in tenorite, copper is 4-fold coordinated with two additional axial O atoms at equivalent distances exhibiting the characteristic Jahn-Teller distortion, in spertiniite, copper is 5-fold coordinated (square pyramidal), with an additional axial oxygen at a greater distance. While both model compounds capture the main feature (**I**), related to the 4 equatorial oxygens (O_{eq}), and part of the remaining spectra, fitting the details of the remaining features are very much dependent of the model used. Therefore, apart from using each model compound separately, a combination of O_{eq} from $Cu(OH)_2$ with O_{ax} from CuO was also tested. However, the fits derived using CuO as model compound are generally poorer, a similar result to that previously obtained by Brigatti *et al.* (2004). Using the tenorite model would imply assigning feature **III** mostly to the Cu first shell, while the signal due to the axial

oxygens should be shifted towards the right at slightly higher distances, which means that at low Cu coverages that feature should be absent or much depressed in the collected spectra. Therefore, the coordination environment of copper in spertiniite provides the best initial trial structure for fitting the obtained spectra, an aspect that even the mixed models used did not improve noticeably. The results of the best fits with spertiniite are summarized in Fig. 4 and Table 1. These show that copper atoms were determined to have four O atoms at average distances of 1.95(1) Å, indicating that Cu-O_{eq} is 4-fold. The use of spertiniite as a basis for the fitting allowed us to distinguish two independent O atoms that form Cu-O_{ax} at average distances of 2.32(16) and 3.06(9) Å. The latter value generally decreases with higher % Cu, having initially an average distance of 3.11(8) Å, which then reduces to 2.97(2) Å above circa 0.5 wt%. Furthermore, the inclusion of copper oligomers to the structural models were seen to make an improvement to the fit for % Cu above circa 1 wt%, having a coordination of 2 and average Cu-Cu distance of 3.10(2) Å.

3.4. *ab initio* calculations

Accordingly with EXAFS spectra fitting and modelling results, the $Cu(H_2O)_5$ geometry was optimized and yielded elongated square pyramidal structures. Inclusion of implicit solvent model led only to a very small decrease of the Cu-O distances by 0.01 Å (Fig. 5; Table S3 in SI file). The square pyramidal geometry for Cu^{2+} in aqueous solution was modelled by Liu et al. (2015) in their study of Cu redox potential, a geometry that was further confirmed by La Penna et al. (2015) in their calculation of Cu^{2+} XANES spectra. However, Frank et al. (2015) provided a combined theoretical and experimental (EXAFS) study of Cu^{2+} speciation in aqueous solution. Therefore, following the approach of Frank and co-workers on $Cu(H_2O)_5 + H_2O$, geometry optimizations were performed with the extra water molecule starting at 2.3 and 3.3 Å from the copper atom.

This enabled us to include the minima proposed by the EXAFS performed by Frank *et al.* (2015) on aqueous solutions (l), and also at 2.8 Å to include a mid-point, whereby the sixth water molecule was added in an axial position at the different distances indicated and hence starting the calculations with a coordination shell of six. In the gas phase (g), the geometries obtained for the extra water molecule starting at 2.8 and 3.3 Å were identical, optimizing to elongated square pyramidal configuration while the structure with an extra water molecule starting at 2.3 Å optimized to a Jahn-Teller octahedral (Fig. 5). The energy of the octahedral was approximately 17 kJ/mol less stable than the 5-fold configuration (elongated square pyramidal). In aqueous conditions all starting configurations revert to the elongated square pyramidal configuration with 4-fold average distance of Cu-O_{eq} equal to 1.97(1) Å, and Cu-O_{ax} of 2.20 Å and 3.63 Å, where the latter is from a non-bonded water molecule. Other charged clusters such as the $Cu(OH)_2(H_2O)_4$ trans structure studied by Bryantsev *et al.* (2009) lead to the square planar geometry.

4. DISCUSSION

It has been widely shown that adsorption phenomena (*i.e.* ions and molecules) onto mineral surfaces depend on the pH of the solution, with the surface adsorption capacity of cations, such as copper, increasing as pH increases. The reason is clear, as shown in Fig. S9, since the number of negatively charged surface sites increases with pH. But phyllosilicates, whose (001) basal surface bears a permanently negative charge can make this simple observation more complicated than it seems. Changing background electrolyte concentration can lead to changes in total adsorption capacity, and dynamics between outer-sphere and inner-sphere complex formation, such as in Co and Pb on montmorillonite (Papelis and Hayes, 1996; Strawn and Sparks, 1999). However,

Tournassat et al. (2013) points out the importance of ionic strength selection in constraining the information on surface charge and site availability. Morton *et al.* (2001) found increasing adsorption onto the (001) sites on montmorillonite as the background electrolyte concentration of the solution tended towards zero. Therefore, it would require a wide range of background electrolyte concentration to properly assess its influence on materials used. Thus, this systematic study of copper adsorption on illite focus on the range of pH values in order to identify mechanisms and structural configurations prevailing in copper adsorption onto illite surfaces.

4.1 Batch experiments

The batch experiments suggest two different mechanisms for copper sorption at pH of 5.5 or below, and pH of 6.5. According to speciation modeling results (Fig. S9) it is inferred that adsorption at pH 4.5 and 5.5 is dominated by the formation of a copper surface complex at the expense of the hydrated Cu^{2+} in solution, namely $\equiv SOCu^{+}$ and very marginally the complex $\equiv SOCuOH$. We can ascertain that illite adsorbs significantly more copper at pH 5.5 than at pH 4.5 (80-100% more using averaged values), which agrees with the speciation modeling and also with what is generally observed in similar systems (Gonçalves, 2006).

As previously noted, using Du et al. (1997b) model of the adsorption equilibrium of copper onto illite surfaces combined with their illite surface chemical properties (Du et al., 1997a), provided very good results for explaining the adsorption behavior of Cu in the batch experiments for EXAFS analysis. This is not the only illite surface speciation model available, but using Bradbury and Baeyens (2009) surface protonation-deprotonation constants as an alternative framework gave different results, with substantially less Cu adsorbed predicted at pH 4.5 and noticeable less at pH 5.5 than obtained in our preparation experiments. Alternatively, the model of Alvarez-Puebla et

al. (2005), a linear combination of 2 Langmuir isotherms (lower and higher pH) and one Freundlich isotherm for the precipitated phase, underestimates Cu adsorption at pH 4.5 and 5.5 as compared with experimental data (Fig. S10 and S11), noting that at pH 5.5 their linear model must be truncated because the function is unbounded at high Cu concentrations. However, the observed conditions for Cu hydroxide precipitation in the model of Alvarez-Puebla et al. (2005) are at odds with our own experimental data. This means that if the final Freundlich term is eliminated altogether at the fitted conditions close to pH 4.5 and 5.5, we get an acceptable approximation that slightly underestimates our experimental data for the concentration range used (Fig. S11), but fails for pH 6.5 because it is controlled by precipitation and the model last term. It should be noted that Du's model does not consider outer-inner sphere complex distinction, a feature that certainly would have a role in the proper description of the Cu-solution-mineral system, and already outlined by other researchers (e.g. Peacock and Sherman, 2004; Zhang *et al.*, 2017). The contribution of the ≡SOCuOH surface complex is only marginal and mainly at pH 5.5. However, using a slight different log K for the formation of $\equiv SOCu_2(OH)^{2+}$ (referred as Model 2 in Fig. 1) improves fitting at pH 6.5 with still acceptable fits for the remaining pH values. Without this change part of the adsorption at pH 4.5 would be better explained by a combination with cation exchange (Fig. 1), which could also be supported by some published results under similar experimental conditions which are extensively reviewed by Tournassat et al. (2013).

The linear increase in adsorbed copper as solution copper concentration increases observed at pH 6.5 is highly suggestive of a different mechanism, which as will be argued later, is mainly controlled by Cu surface precipitation. However, other possibilities can potentially explain the measured adsorbed copper in solutions at pH 6.5 as being significantly higher than at lower pH, and thus we will start arguing why these

hypotheses can be ruled out. At the highest copper concentrations used in the starting solution (10^{-3} M) at pH 6.5 copper hydroxide ($Cu(OH)_2$) is slightly supersaturated (calculated saturation index is 0.44 as seen in Fig. S8) and thus it may potentially precipitate. However, once copper is added to the reactor solution it quickly adsorbs onto the suspended illite, and thus the saturation index of copper hydroxide is likely to drop significantly. Additionally, if copper hydroxide had precipitated out of the solution, and because pH was always monitored for correction after 12 h, we should have observed a significant pH drop in the solution inside the reactors. Direct copper hydroxide precipitation is thus ruled out because no significant pH drop was registered in these experiments, and so most probably the rapid adsorption of copper onto the illite surface depresses the saturation index of $Cu(OH)_2$ so much that prevents crystal nucleation and precipitation, sustaining undersaturated conditions. Formation of surface carbonate complexes can be an understandable concern at higher pH because the solutions in the batch experiments were in equilibrium with the atmosphere. However, because Du et al. (1997b) while studying their system used a wide range of pH up to 9, needed to account for carbonate complex formation and in fact identified surface carbonate species using FTIR (a feature we didn't identify in the collected spectrum, see Fig. S3). Furthermore, the simulations show that in order to have significant carbonate species present, pH values in excess of 7 would be required (Fig. S8), which was not attained in our experiments. So, we conclude that there was no carbonate effect in the experiments, or at most may be so marginally small that remained undetected.

Ruling out these hypotheses leads to the effects of surface Cu precipitation and simulating the surface Cu hydroxide species of Du's model as a phase indicates that it starts forming at Cu solution concentrations in excess of 18 mg/l (0.28 mM) in equilibrium with adsorbed Cu on illite, explaining the sudden increase in Cu uptake at

higher solution concentrations (Fig. 1c). The other aspect to properly explain the experimental data is the use of the CD-MUSIC surface complexation model at pH 6.5, which seems to suggest that more than one surface site may be active in Cu adsorption. This result can be assigned to the surface charge distribution assumed in this model.

4.2 EXAFS experiments

The evaluation of EXAFS spectra (Fig. 2 and 3) have shown that the equatorial oxygen (O_{eq}) atoms have a dominant effect in features **I**, **II** and **III** (the last one in the case of model spertiniite only), as it has been previously seen in montmorillonite and kaolinite samples (*e.g.* Schlegel and Manceau (2013)). We found that features **II** and **III** were also linked with axial oxygen atoms (O_{ax}) and their relative positions. The use of both spertiniite ($Cu(OH)_2$) and tenorite (CuO) as model compounds in the fitting procedure, also made apparent that feature **IV**, and to a smaller extent also **III** are related to Cu-Cu interactions. In tenorite, the signal of the first Cu-Cu shell would shift the spectra towards feature **III**. So the details of the fitting of feature **III** on our experimental data provides the distinction in considering it the result of the first Cu shell (as in tenorite) or the signal from the distant axial oxygen as seen in spertiniite, which has given better fits and more realistically coordination environments for the formation of Cu oligomers as will be discussed later.

Analysis of the EXAFS data led to the widely accepted 4-fold coordinated Cu-O_{eq} (1.95(1) Å). The Cu-O_{ax} presented a bimodal distance distribution with bond lengths of 2.32(16) and 3.06(9) Å (Fig. S6); the latter changed as a function of % Cu, decreasing from 3.11(8) Å for % Cu below 0.5% to 2.97(2) Å above such value. This trend with increasing % Cu is clearly seen as the pH increases, being less obvious at pH 4.5 although a distance at 3.04 Å has been fitted. Modelling of batch experiments at pH 6.5 and higher copper content indicates the presence of copper surface precipitates (Fig. S9)

which is accompanied by the clear enhance of feature **IV** and almost disappearance of feature **III** (Fig. 2), thus leading us to test the inclusion of copper oligomers in the EXAFS fits at higher % Cu, and again compatible with the spertiniite spectrum. With copper content higher than 1% Cu, which is only obtained in the pH 6.5 experiments, the Cu-Cu distance obtained was on average 3.10(2) Å. These results are consistent with copper dimers and trimers with Cu-Cu distances around 3 Å, in montmorillonite (Brigatti et al., 2004; Morton et al., 2001), kaolinite (Peacock and Sherman, 2005b), and Goethite, Hematite, and Lepidocrocite (Peacock and Sherman, 2004). Therefore, these Cu-Cu distances are concurrent with the formation of a surface precipitate, that has the structural characteristics of a Cu hydroxide phase, most likely the $\equiv SOCu_2(OH)_3(sp)$ surface precipitate predicted by Du's model.

When considering the Cu-O distances we obtained from EXAFS up to 3 Å (Hathaway, 1987), is suggestive of a five-fold first coordination shell for copper for % Cu below 0.5% or lower pH (at least < 5.5). At higher copper content the Cu-O bond lengths are commensurate with six-fold coordination environment. Furthermore, the Cu-O distances obtained from our EXAFS fitting agree well with previous work on copper coordination in solution *i.e.* elongated square pyramidal and Jahn-Teller octahedral structures (Pasquarello *et al.*, 2001; Persson *et al.*, 2002; Schwenk and Rode, 2003; Burda *et al.*, 2004; Frank *et al.*, 2005; Chaboy *et al.*, 2006; Bryantsev *et al.*, 2008; Bryantsev *et al.*, 2009; Ames and Larsen, 2009; Liu *et al.*, 2010; Gomez-Salces *et al.*, 2012; Frank *et al.*, 2015; Zhang *et al.*, 2017).

The non-bonded character of the longest EXAFS Cu-O_{ax} (3.11(8) Å) may be viewed as the result of a weaker bonding to the surface. The review by Tournassat et al. (2013) on adsorption of divalent metals on montmorillonite surfaces may provide some insight to interpret our results. According to these authors, cation exchange is the dominant

mechanism in low ionic strength solutions ($\leq 10^{-3}$ M), while the model of Alvarez-Puebla et al. (2005) considering the pH, finds a somewhat similar conclusion at low pH (4 – 4.5). Therefore, using 10^{-3} M concentration of a background electrolyte the conditions for the adsorption experiments would indicate cation exchange as the main adsorption mechanism, but since it develops onto the (001) permanently charged clay surfaces, means that Cu adsorption would be pH independent, and we observe differences between pH 4.5 and 5.5 experiments and in EXAFS data. However, Morton et al. (2001) and Papelis and Hayes (1996) found such evidence for infinitely diluted solutions and unchanged adsorption behaviour with pH, respectively. So, we cannot dismiss cation exchange entirely, which may partially lend some credit to the low pH adsorption models of Alvarez-Puebla et al. (2005) or even to part of our SCM at pH 4.5. Since EXAFS spectra is an average probe of the signal of adsorbed Cu on the illite surface, these longer Cu-O_{ax} distances may be probing more than a single mechanism, possibly cation exchange and outer-sphere-type complex, because both represent weakly bond complexes on the surface, at low copper content (below 0.5% Cu).

The decrease in the average Cu-O_{ax} distance to 2.97(2) Å at copper loads greater than 0.5% Cu (and increasing pH) indicates a stronger bonding character for the surface copper complex, which may be linked to the increased affinity for different edge sites. Again, Tournassat et al. (2013) provide in their review of the published literature that at least in montmorillonite these changing conditions activate low and high energy sites (LES and HES, respectively). So, HES are also high affinity sites that likely control adsorption at high ionic strength and low metal equilibrium concentration. Increasing metal solution concentration saturates HES and activates adsorption on LES. These situations have been observed by Dähn et al. (2011) and later modelled by Churakov and Dähn (2012) for Zn in montmorillonite, and more recently by Zhang *et al*, (2017).

The model of Bradbury and Baeyens (2009) is the only providing more than one surface affinity site for illite, but the use of Du's Cu surface complexation model gave very good fits to the experimental results in all experiments. Nevertheless, as noted before, at pH 6.5 the use of the DDL model provided a poor fit to the experimental results, and the corresponding improvement with CD-MUSIC may well suggest that at higher pH and increasing Cu loads more than a single site activates, which according to Tournassat et al. (2013) would mean both HES and LES. It is worth noting that at pH 6.5 with the lowest Cu loads, Cu-O_{ax} is 3.01 Å, at about the same distance or even less than at higher Cu loads and pH 4.5 and 5.5. Whether this may also represent a transition towards an inner-sphere-type complex is uncertain, but surely advocates for a stronger binding to the illite surface.

Finally, our finding that the Cu-Cu distance is 3.10(2) Å, at % Cu above 1% and pH 6.5, is very well correlated with the Al-Al distances of the edge surfaces from the octahedral sheet (Martins et al., 2014), suggesting that higher copper loads lead towards the epitaxial control on copper deposition. This observation has yet another implication, which is the predominance of the edge surfaces relative to the basal ones in controlling Cu uptake at this pH because of the Cu-Cu and Al-Al distances correlation.

Finally, it should be noted that using first principles molecular dynamics, Zhang at al. (2017) provide the mechanisms of Cu adsorption on 2:1 clay edge sites, suggesting the octahedral vacant site as a HES in the sense of Tournassat et al. (2013) definition. While their study provide a geometrical configuration of the Cu complex in the edge surface, with Cu forming edge-sharing bi-dentate complexes in the Al-sites, it should be stressed that the EXAFS data collected probes an average signal of the bound Cu-complexes on the surface. A similar result is also provided by Yang et al. (2015) using experimental data. Nevertheless, it generally agrees with both our findings of the importance of the

Al-sites and the more likely five-fold coordination for Cu. Therefore, given the correlation of the sixth coordinated oxygen distance with Cu concentration and pH we favour this as showing the changing mechanisms of Cu bonding to the edge surface as pH and Cu concentration increase in aqueous solution.

We therefore postulate that the conversion to the stronger bonding mechanism onto high affinity sites is linked with the appearance of oligomers which in turn lead to more contact points with the illite edge surfaces hence the interaction becomes stronger.

4.3 ab initio calculations

Our DFT calculations predicted both the elongated square pyramidal and Jahn-Teller octahedral coordination geometries, with the former being more stable both in gas and aqueous phases. It should be noted that the $Cu(H_2O)_5 + H_2O$ geometry optimizations in the gas phase yielded both an elongated square pyramidal and Jahn-Teller octahedral configurations, depending on the initial position of the extra water molecule. However, of these the former configuration was also determined to be more stable (by approximately 17 kJ/mol). Being a small value it supports the proposal that both coordination clusters are accessible, agreeing and supporting the EXAFS fits whereby a 5-fold first shell is attained al low % Cu and 6-fold at high % Cu.

In terms of the structure obtained from our simulations at the aqueous environment (closer to the EXAFS experimental conditions), the elongated square pyramidal calculations are in excellent agreement with the data obtained from our best fitting (*e.g.* for the distribution of the $Cu\text{-}O_{ax}$ experimentally averaged to 2.30(18) Å and calculated to be 2.19 Å). We therefore show evidence that the results obtained from our *ab initio* calculations on the copper configurations in aqueous solution have merit in interpreting the structural configuration of this metal in adsorption studies, although models of adsorbed copper on edge surfaces would be even more invaluable.

5. CONCLUSIONS

We have studied copper adsorption on illite samples using a combination of experimental and computational techniques in a systematic approach. In spite the inherent difficulty in interpreting EXAFS data since it depends on the model used for the fitting procedure, a consistent pattern emerged in the Cu-O_{ax} and Cu-Cu distances, in which they are found to be highly correlated with the pH and copper concentration. We found that the elongated square pyramidal configuration is the more likely for the first shell of Cu-water configuration based on the fits obtained to the EXAFS data, which was corroborated by our *ab initio* calculations. Use of large scale molecular modelling based on molecular dynamics may thus usefully explore whether there is a dynamic equilibration in the coordination of the clusters. EXAFS data analysis suggests that copper initially adsorbs onto illite surfaces establishing weaker bonds, possibly due to a combination of surface complexation and cation exchange at lower pH, based on the characteristic of the Cu-O_{ax} distances and supported by surface complexation modelling. As these distances decrease with increasing copper concentration, we infer that the adsorption mechanism changes favouring high affinity edge surface sites. At high pH and copper content, there is the formation of copper oligomers at the surfaces of illite. The geometry of the adsorbed oligomers is governed by the edge surfaces based on the correlation of the Cu-Cu and Al-Al distances. We have critically assessed the models used for the fitting of EXAFS data and infer that although models based on aqueous copper still give valuable results, structural models based on copper adsorbed at edge surface of clay should be considered in order to clarify some of the persisting incongruences in these models. Future work is due in characterizing the adsorption sites and processes on the edge surfaces via atom level simulation.

ACKNOWLEDGEMENTS

The authors would like to thank the financial support of the FCT ("Fundação para a Ciência e a Tecnologia") under the KADRWaste Grant - PTDC/CTE-GEX/82678/2006, the Department of Geology of the University of Lisbon and the Synchrotron Light Source ANKA for provision of beamtime at the SUL-X beamline within the proposal ENV-206. Publication supported by FCT project UID/GEO/50019/2013 - Instituto Dom Luiz. D.M.S.M. also acknowledges the FCT for the award of a post-doctoral fellowship (SFRH/BPD/71118/2010). The authors also wish to acknowledge the comments and criticisms provided by two anonymous referees who helped improve our manuscript.

APPENDIX A. SUPPLEMENTARY DATA

Supplementary data associated with this article can be found, in the online version.

REFERENCES

Alvarez-Puebla, R. A., Santos Jr., D. S., Blanco, C., Echevarria, J, C. and Garrido, J. J. (2005) Pasrticle and surface charcaterization of a natural illite and study of its copper retention, Journal of Colloid and Interface Science, 285, 41-49.

Ankudinov, A.L., Ravel, B., Rehr, J.J. and Conradson, S.D. (1998) Real-space multiple-scattering calculation and interpretation of x-ray-absorption near-edge structure. Physical Review B 58, 7565-7576.

Ames, W. M. and Larsen, S. C. (2009) Density Functional Theory Investigation of EPR Parameters for Tetragonal Cu(II) Model Complexes with Oxygen Ligands. Journal of Physical Chemistry A, 113, 4305-4312.

Becke, A.D. (1993) Density-functional thermochemistry. III. The role of exact exchange. The Journal of Chemical Physics 98, 5648-5652.

Berti, W.R. and Jacobs, L.W. (1996) Chemistry and Phytotoxicity of Soil Trace Elements from Repeated Sewage Sludge Applications. Journal of Environmental Quality 25, 1025-1032.

Bradbury, M. H. and Baeyens, B. (2009) Sorption modelling on illite Part I: Titration measurements and the sorption of Ni, Co, Eu and Sn, Geochimica et Cosmochimica Acta, 73, 990-1003.

Bradl, H.B. (2004) Adsorption of heavy metal ions on soils and soils constituents. J. Colloid Interface Sci. 277, 1-18.

Brigatti, M.F., Colonna, S., Malferrari, D. and Medici, L. (2004) Characterization of Cu-complexes in smectite with different layer charge location: Chemical, thermal and EXAFS studies. Geochim. Cosmochim. Acta 68, 781-788.

Bryantsev, V.S., Diallo, M.S. and Goddard, W.A. (2009) Computational Study of Copper(II) Complexation and Hydrolysis in Aqueous Solutions Using Mixed Cluster/Continuum Models. Journal of Physical Chemistry A 113, 9559-9567.

Bryantsev, V.S., Diallo, M.S., van Duin, A.C.T. and Goddard Iii, W.A. (2008) Hydration of Copper(II): New Insights from Density Functional Theory and the COSMO Solvation Model. The Journal of Physical Chemistry A 112, 9104-9112.

Burda, J.V., Pavelka, M. and Simanek, M. (2004) Theoretical model of copper Cu(I)/Cu(II) hydration. DFT and ab initio quantum chemical study. J Mol Struc-Theochem 683, 183-193.

Calos, N.J., Forrester, J.S. and Schaffer, G.B. (1996) A Crystallographic Contribution to the Mechanism of a Mechanically Induced Solid State Reaction. Journal of Solid State Chemistry 122, 273-280.

Cances, E., Mennucci, B. and Tomasi, J. (1997) A new integral equation formalism for the polarizable continuum model: Theoretical background and applications to isotropic and anisotropic dielectrics. Journal of Chemical Physics 107, 3032-3041.

Chaboy, J., Munoz-Paez, A., Merkling, P.J. and Marcos, E.S. (2006) The hydration of Cu2+: Can the Jahn-Teller effect be detected in liquid solution? Journal of Chemical Physics 124.

Cheah, S.F., Brown, G.E. and Parks, G.A. (1998) XAFS spectroscopy study of Cu(II) sorption on amorphous SiO2 and gamma-Al2O3: Effect of substrate and time on sorption complexes. J. Colloid Interface Sci. 208, 110-128.

Chen, C.C. and Hayes, K.F. (1999) X-ray absorption spectroscopy investigation of aqueous Co(II) and Sr(II) sorption at clay-water interfaces. Geochim. Cosmochim. Acta 63, 3205-3215.

Churakov, S. V. and Dähn, R. Zinc adsorption on clays inferred from atomistic simulations and EXAFS spectroscopy, Environmental Science and Technology, 46, 5713-5719.

Dähn, R., Scheidegger, A.M., Manceau, A., Schlegel, M.L., Baeyens, B., Bradbury, M.H. and Chateigner, D. (2003) Structural evidence for the sorption of Ni(II) atoms on the edges of montmorillonite clay minerals: a polarized X-ray absorption fine structure study. Geochim. Cosmochim. Acta 67, 1-15.

Dähn, R., Baeyens, B. and Bradbury, M. H. (2011) Investigation of the different binding edge sites for Zn in montmorillonite using P-EXAFS: The strong/weak site concept in the 2SPNE SC/CE soprtion model, Geochimica et Cosmochimica Acta, 75, 5154-5168.

Du, Q., Sun, Z.X., Forsling, W. and Tang, H.X. (1997a) Acid–Base Properties of Aqueous Illite Surfaces. J. Colloid Interface Sci. 187, 221-231.

Du, Q., Sun, Z.X., Forsling, W. and Tang, H.X. (1997b) Adsorption of copper at aqueous illite surfaces. J. Colloid Interface Sci. 187, 232-242.

Egirani, D.E., Baker, A.R. and Andrews, J.E. (2005) Copper and zinc removal from aqueous solution by mixed mineral systems I. Reactivity and removal kinetics. J. Colloid Interface Sci. 291, 319-325.

Farquhar, M.L., Vaughan, D.J., Hughes, C.R., Charnock, J.M. and England, K.E.R. (1997) Experimental studies of the interaction of aqueous metal cations with mineral substrates: Lead, cadmium, and copper with perthitic feldspar, muscovite, and biotite. Geochim. Cosmochim. Acta 61, 3051-3064.

Figueiras, J., Goncalves, M.A., Mateus, A., Marques, F.O., Santos, F.M. and Mota, R. (2009) Initial stages of pollutants dispersion around municipal waste disposal facilities: A case study in Northern Portugal. International Journal of Environment and Waste Management 4, 341-365.

Flogeac, K., Guillon, E. and Aplincourt, M. (2004) Surface Complexation of Copper(II) on Soil Particles: EPR and XAFS Studies. Environ. Sci. Technol. 38, 3098-3103.

Frank, P., Benfatto, M., Szilagyi, R.K., D'Angelo, P., Longa, S.D. and Hodgson, K.O. (2005) The Solution Structure of [Cu(aq)]2+ and Its Implications for Rack-Induced Bonding in Blue Copper Protein Active Sites. Inorganic Chemistry 44, 1922-1933.

Frank, P., Benfatto, M., Qayyam, M., Hedman, B. and Hodgson, K.O. (2015) A high-resolution XAS study of aqueous Cu(II) in liquid and frozen solutions: Pyramidal, polymorphic, and non-centrosymmetric. The Journal of Chemical Physics 142, 084310.

Frisch, M.J., Pople, J.A. and Binkley, J.S. (1984) Self-consistent molecular orbital methods 25. Supplementary functions for Gaussian basis sets. The Journal of Chemical Physics 80, 3265-3269.

Frisch, M.J., Trucks, G.W., Schlegel, H.B., Scuseria, G.E., Robb, M.A., Cheeseman, J.R., Montgomery, J.A., Vreven, T., Kudin, K.N., Burant, J.C., Millam, J.M., Iyengar, S.S., Tomasi, J., Barone, V., Mennucci, B., Cossi, M., Scalmani, G., Rega, N., Petersson, G.A., Nakatsuji, H., Hada, M., Ehara, M., Toyota, K., Fukuda, R., Hasegawa, J., Ishida, M., Nakajima, T., Honda, Y., Kitao, O., Nakai, H., Klene, M., Li, X., Knox, J.E., Hratchian, H.P., Cross, J.B., Bakken, V., Adamo, C., Jaramillo, J., Gomperts, R., Stratmann, R.E., Yazyev, O., Austin, A.J., Cammi, R., Pomelli, C., Ochterski, J.W., Ayala, P.Y., Morokuma, K., Voth, G.A., Salvador, P., Dannenberg, J.J., Zakrzewski, V.G., Dapprich, S., Daniels, A.D., Strain, M.C., Farkas, O., Malick, D.K., Rabuck, A.D., Raghavachari, K., Foresman, J.B., Ortiz, J.V., Cui, Q., Baboul, A.G., Clifford, S., Cioslowski, J., Stefanov, B.B., Liu, G., Liashenko, A., Piskorz, P., Komaromi, I., Martin, R.L., Fox, D.J., Keith, T., Laham, A., Peng, C.Y., Nanayakkara, A., Challacombe, M., Gill, P.M.W., Johnson, B., Chen, W., Wong, M.W., Gonzalez, C. and Pople, J.A. (2003) Gaussian 03, Revision C.02.

Gier, S. and Johns W. D. (2000) Heavy metal-adsorption on micas and clay minerals studied by X-ray photoelectron spectroscopy, Applied Clay Science, 16, 289-299.

Gomez-Salces, S., Aguado, F., Valiente, R. and Rodrigues, F. (2012) Unraveling the Coordination Geometry of Copper(II) Ions in Aqueous Solution through Absorption Intensity. Angewandte Chemie-International Edition 51, 9335-9338.

Gonçalves, M.A. (2006) Adsorption of Cu onto illite surfaces: Kinetics and Metal-Organic acid interactions, XXVI REUNiÓN (SEM) / XX REUNiÓN (SEA) Macla, pp. 233-236.

Gonçalves, M.A., Nogueira, J.M.F., Figueiras, J., Putnis, C.V. and Almeida, C. (2004) Base-metals and organic content in stream sediments in the vicinity of a landfill. Applied Geochemistry 19, 137-151.

Hathaway, B.J. (1987) in: Wilkinson, G. (Ed.), Comprehensive Coordination Chemistry. Pergamon, Oxford, vol. 5, pp. 533-774.

Hesterberg, D., Sayers, D.E., Zhou, W., Robarge, W.P. and Plummer, G.M. (1997) XAFS characterization of copper in model aqueous systems of humic acid and illite. J. Phys. IV 7, 833-834.

Hiesmtra, T. and Van Reimsdijk (1996) A surface structural approach to ion adsorption: the charge distribution (CD) model. Journal of Colloid and Interface Science, 179, 488-508.

Hower, J. and Mowatt, T.C. (1966) Mineralogy of illites and mixed-layer illite/montmorillonites. Am. Miner. 51, 825-854.

Hyun, S.P., Cho, Y.H., Kim, S.J. and Hahn, P.S. (2000) Cu(II) sorption mechanism on montmorillonite: An electron paramagnetic resonance study. J. Colloid Interface Sci. 222, 254-261.

Hyun, S.P. and Hayes, K.F. (2015) X-ray absorption spectroscopy study of Cu(II) coordination in the interlayer of montmorillonite. Applied Clay Science 107, 122-130.

Kerisit, S. and Parker, S.C. (2004) Free Energy of Adsorption of Water and Metal Ions on the $\{10\bar{1}4\}$ Calcite Surface. J. Am. Chem. Soc. 126, 10152-10161.

Krishnan, R., Binkley, J.S., Seeger, R. and Pople, J.A. (1980) Self-consistent molecular-orbital methods .20. Basis set for correlated wave-functions. Journal of Chemical Physics 72, 650-654.

La Penna, G., Minicozzi, V., Morante, S., Rossi, G. C. amd Stellato, F. (2015) A first-principle calculation of the XANES spectrum of Cu^{2+} in water. Journal of Chemical Physics 143, 124508.

Lee, C., Yang, W. and Parr, R.G. (1988) Development of the Colle-Salvetti correlation-energy formula into a functional of the electron density. Physical Review B 37, 785-789.

Liu, X., Lu, X., Jan Meijer, E. and Wang, R. (2010) Hydration mechanisms of Cu2+: tetra-, penta- or hexa-coordinated? Phys. Chem. Chem. Phys. 12, 10801-10804.

Liu, X., Chang, J. and Sprik, M. (2015) Aqueous transition-metal cations as impurities in a Wide Gap Oxide: the Cu^{2+}/Cu^{+} and Ag^{2+}/Ag^{+} redox couples revisited. Journal of Physical Chemistry B, 119, 1152-1163.

Madrid, L. and Díaz-Barrientos, E. (1998) Release of metals from homogeneous soil columns by wastewater from an agricultural industry. Environmental Pollution 101, 43-48.

Martins, D.M.S., Middlemiss, D.S., Pulham, C.R., Wilson, C.C., Weller, M.T., Henry, P.F., Shankland, N., Shankland, K., Marshall, W.G., Ibberson, R.M., Knight, K., Moggach, S., Brunelli, M. and Morrison, C.A. (2009) Temperature- and Pressure-induced Proton Transfer in the 1:1 Adduct Formed between Squaric Acid and 4,4 '-Bipyridine. Journal of the American Chemical Society 131, 3884-3893.

Martins, D.M.S., Molinari, M., Goncalves, M.A., Mirao, J.P. and Parker, S.C. (2014) Toward Modeling Clay Mineral Nanoparticles: The Edge Surfaces of Pyrophyllite and Their Interaction with Water. J. Phys. Chem. C 118, 27308-27317.

McLean, A.D. and Chandler, G.S. (1980) Contracted gaussian-basis sets for molecular calculations .1. 2nd row atoms, z=11-18. Journal of Chemical Physics 72, 5639-5648.

Mellouk, S., Belhakem, A., Marouf-Khelifa, K., Schott, J. and Khelifa, A. (2011) Cu(II) adsorption by halloysites intercalated with sodium acetate. J. Colloid Interface Sci. 360, 716-724.

Mennucci, B., Cances, E. and Tomasi, J. (1997) Evaluation of solvent effects in isotropic and anisotropic dielectrics and in ionic solutions with a unified integral equation method: Theoretical bases, computational implementation, and numerical applications. Journal of Physical Chemistry B 101, 10506-10517.

Mennucci, B. and Tomasi, J. (1997) Continuum solvation models: A new approach to the problem of solute's charge distribution and cavity boundaries. Journal of Chemical Physics 106, 5151-5158.

Morton, J.D., Semrau, J.D. and Hayes, K.F. (2001) An X-ray absorption spectroscopy study of the structure and reversibility of copper adsorbed to montmorillonite clay. Geochim. Cosmochim. Acta 65, 2709-2722.

Oswald, H.R., Reller, A., Schmalle, H.W. and Dubler, E. (1990) Structure Of Copper(II) Hydroxide, Cu(OH)2. Acta Crystallogr. Sect. C-Cryst. Struct. Commun. 46, 2279-2284.

Papelis, C. and Hayes, K.F. (1996) Distinguishing between interlayer and external sorption sites of clay minerals using X-ray absorption spectroscopy. Colloids and Surfaces a-Physicochemical and Engineering Aspects 107, 89-96.

Pasquarello, A., Petri, I., Salmon, P.S., Parisel, O., Car, R., Tóth, É., Powell, D.H., Fischer, H.E., Helm, L. and Merbach, A.E. (2001) First Solvation Shell of the Cu(II) Aqua Ion: Evidence for Fivefold Coordination. Science 291, 856-859.

Peacock, C.L. and Sherman, D.M. (2004) Copper(II) sorption onto goethite, hematite and lepidocrocite: a surface complexation model based on ab initio molecular geometries and EXAFS spectroscopy. Geochim. Cosmochim. Acta 68, 2623-2637.

Peacock, C.L. and Sherman, D.M. (2005a) Erratum to Caroline L. Peacock and David M. Sherman (2004) "Copper(II) sorption onto goethite, hematite, and lepidocrocite: A surface complexation model based on ab initio molecular geometries and EXAFS spectroscopy", Geochimica et Cosmochimica Acta 68, 2623–2637. Geochim. Cosmochim. Acta 69, 5141-5142.

Peacock, C.L. and Sherman, D.M. (2005b) Surface complexation model for multisite adsorption of copper(II) onto kaolinite. Geochim. Cosmochim. Acta 69, 3733-3745.

Persson, I., Persson, P., Sandstrom, M. and Ullstrom, A.-S. (2002) Structure of Jahn-Teller distorted solvated copper(ii) ions in solution, and in solids with apparently regular octahedral coordination geometry. Journal of the Chemical Society, Dalton Transactions, 1256-1265.

Ravel, B. and Newville, M. (2005) ATHENA, ARTEMIS, HEPHAESTUS: data analysis for X-ray absorption spectroscopy using IFEFFIT. J. Synchrot. Radiat. 12, 537-541.

Saijdu, S. M. I., Persson, I., Masamba, W. R. L. and Henry, E. M. T. (2008) Mechanisms of heavy metal sorption on alkaline clays from Tundulu in Malawi as determined by EXAFS, Journal of Hazardous Materials, 158, 401-409.

Sanchez, A.G., Ayuso, E.A. and De Blas, O.J. (1999) Sorption of heavy metals from industrial waste water by low-cost mineral silicates. Clay Minerals 34, 469-477.

Scheidegger, A.M., Strawn, D.G., Lamble, G.M. and Sparks, D.L. (1998) The kinetics of mixed Ni-Al hydroxide formation on clay and aluminum oxide minerals: A time-resolved XAFS study. Geochim. Cosmochim. Acta 62, 2233-2245.

Schlegel, M.L. and Manceau, A. (2006) Evidence for the nucleation and epitaxial growth of Zn phyllosilicate on montmorillonite. Geochim. Cosmochim. Acta 70, 901-917.

Schlegel, M.L. and Manceau, A. (2013) Binding mechanism of Cu(II) at the clay-water interface by powder and polarized EXAFS spectroscopy. Geochim. Cosmochim. Acta 113, 113-124.

Schwenk, C.F. and Rode, B.M. (2003) Extended ab initio quantum mechanical/molecular mechanical molecular dynamics simulations of hydrated Cu2+. The Journal of Chemical Physics 119, 9523-9531.

Sherman, D.M. (2009) Surface Complexation Modeling: Mineral Fluid Equilbria at the Molecular Scale, in: Oelkers, E.H., Schott, J. (Eds.), Thermodynamics and Kinetics of Water-Rock Interactions: Reviews in MIneralogy and Geochemistry. The Mineralogical Society of America, vol. 70, pp. 181-205.

Srodon, J. and Eberl, D.D. (1984) Illite, in: Bailey, S.W. (Ed.), Micas. Mineralogical Society of America, Reviews in Mineralogy, vol. 13, pp. 495-544.

Strawn, D.G. and Baker, L.L. (2009) Molecular characterization of copper in soils using X-ray absorption spectroscopy. Environmental Pollution 157, 2813-2821.

Strawn, D.G. and Sparks, D.L. (1999) The use of XAFS to distinguish between inner- and outer-sphere lead adsorption complexes on montmorillonite. J. Colloid Interface Sci. 216, 257-269.

Thompson, H.A., Parks, G.A. and Brown, G.E. (2000) Formation and release of cobalt(II) sorption and precipitation products in aging kaolinite-water slurries. J. Colloid Interface Sci. 222, 241-253.

Tomasi, J., Mennucci, B. and Cances, E. (1999) The IEF version of the PCM solvation method: an overview of a new method addressed to study molecular solutes at the QM ab initio level. J Mol Struc-Theochem 464, 211-226.

Turan, N. G., Elevi, S. and Mesci, B. (2011) Adsorption of copper and zinc ions on illite: Determination of the optimal conditions by the statistical design of experiments, Applied Clay Science, 52, 392-399.

Udiin, M. K. (2017) A review on the adsorption of heavy metals by clay minerals, withspecial focus on the past decade, Chemical Engineering Journal, 308, 438-462.

Vengris, T., Binkiene, R. and Sveikauskaite, A. (2001) Nickel, copper and zinc removal from waste water by a modified clay sorbent. Applied Clay Science 18, 183-190.

Yang, S., Ren, X., Zhao, G., Shi, W., Montavon, G., Grambow, B. and Wang, X. (2015) Competitive sorption and selective sequence of Cu(II) and Ni(II) on montmorillonite: Batch, modeling, EPR and XAS studies, Geochimica et cosmochimica Acta, 166, 129-145.

Zhang, C., Liu, X., Lu, X., Meijer, E. J., Wnag, K., He, M. and Wang, R. (2016) Cadmium(II) complexes adsorbed on clay edge surfaces: insight from first principles molecular dynamics simulation, Clays and Clay Minerals, 64, 335-345.

Zhang, C., Liu, X., Lu, X. He, M., Meijer, E. J. and Wang, R (2017) Surface complexation of heavy metal cations on clay edges: insights from first principles molecular dynamics simulation of Ni(II), Geochimica et Cosmochimca Acta, 203, 54-68.

LIST OF FIGURES

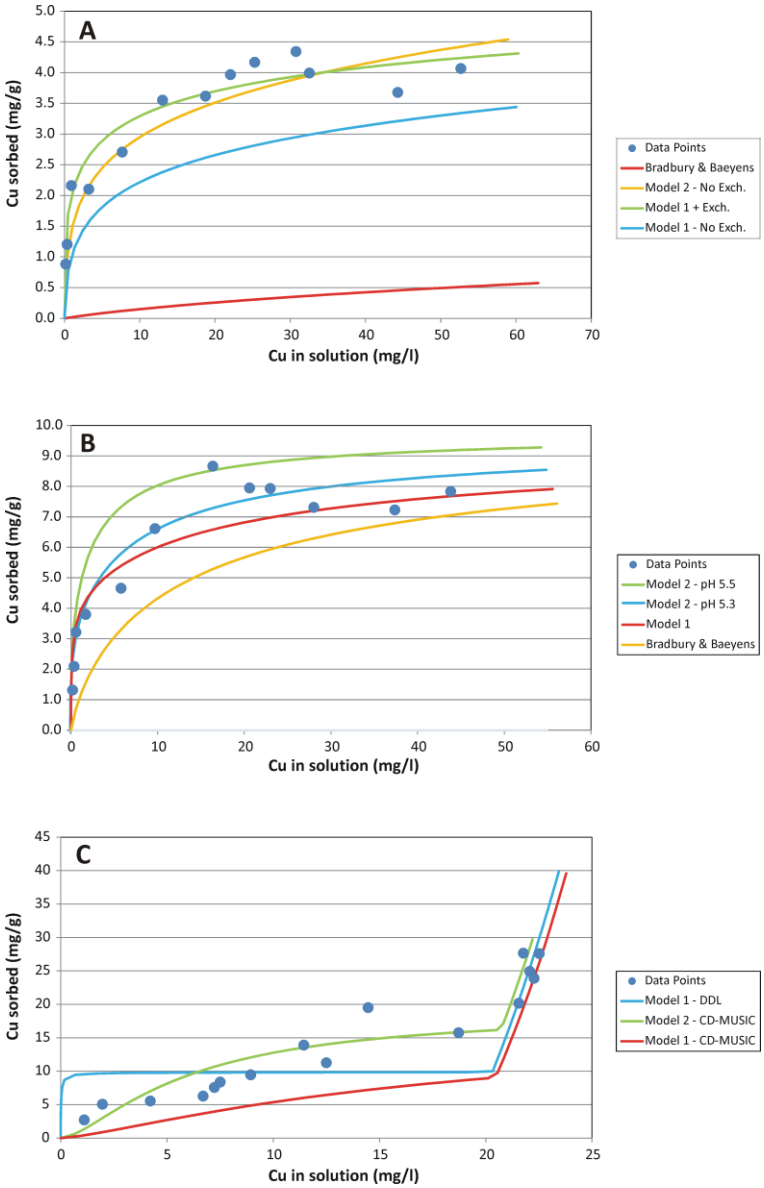

Fig. 1. Results of the batch adsorption experiments with the illites prepared for EXAFS analysis, with fitted models. The models labelled as 1 and 2 are based in Du et al. (1997a; 1997b) and Gonçalves (2006) fitted parameters and Cu speciation model, and are detailed in the SI file. Model 2 changed the surface equilibrium constant of surface reaction 4 (equation 4 in SI) to -11.0, in order to better fit the data at pH 6.5 and used for the remaining pH as well. Also shown are the results using the surface protonation/deprotonation constants of Bradbury and Baeyens (2009) for pH 4.5 and 6.5. **A**: Experiments at pH 4.5 with exchange reaction included in Models 1 and 2 for fitting purposes. **B**: Experiments at pH 5.5 where two pH values (5.5 and 5.3) are used in Model 2 to show the corresponding variation. **C**: Experiments at pH 6.5, where major differences are related to the surface complexation modelling used, DDL – diffuse double layer as in all other models in **A** and **B**, and CD-MUSIC, which provided best fits. All models show the clear onset of surface precipitation at the higher Cu concentrations, which is also clearly indicated by the data.

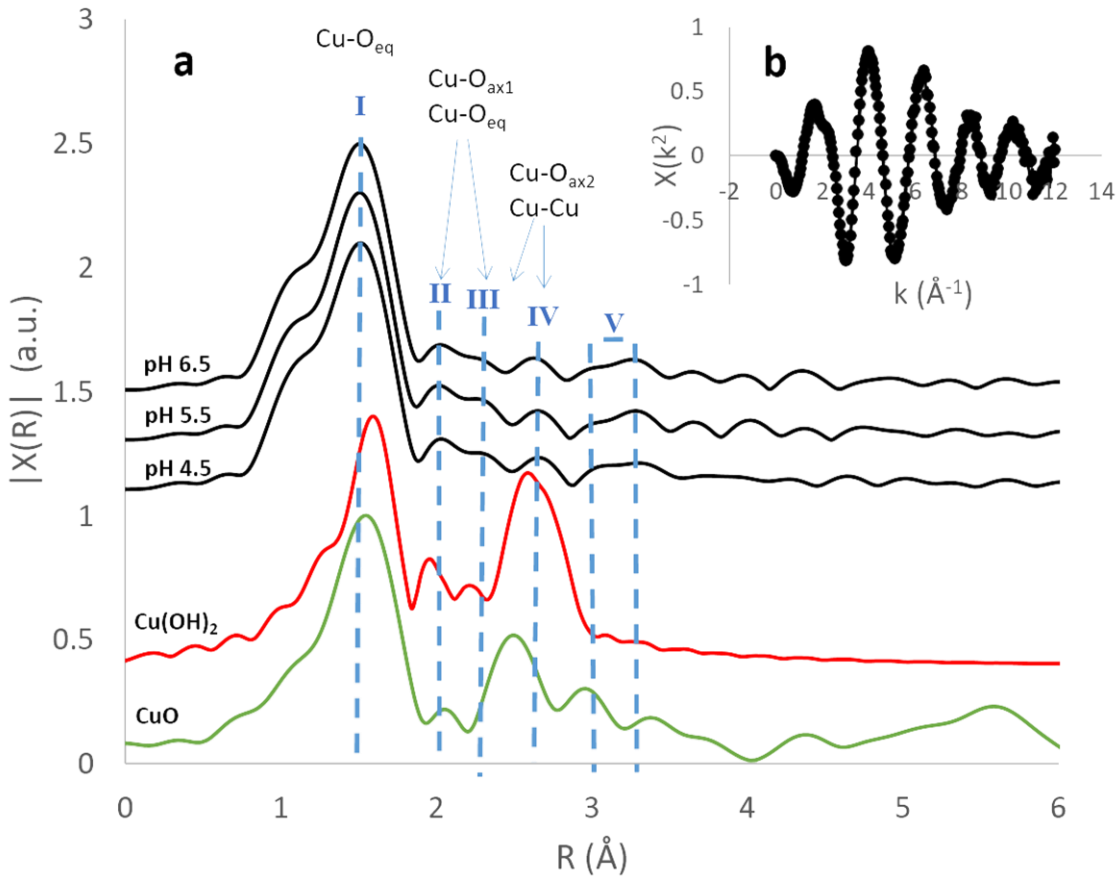

Fig. 2. Cu K-edge EXAFS data for copper adsorbed illites with concentration around 0.35 wt% illite. a) FT and b) associated FT^{-1} scattering curve spectra. Solid black lines are from the experimental data with the respective label for the pH conditions, the solid red line is the experimental spectra for spertiniite ($Cu(OH)_2$), and the solid green line is the experimental spectra for tenorite (CuO). The annotation above the spectra refers the major contributions of each path to the experimental spectrum of spertiniite..

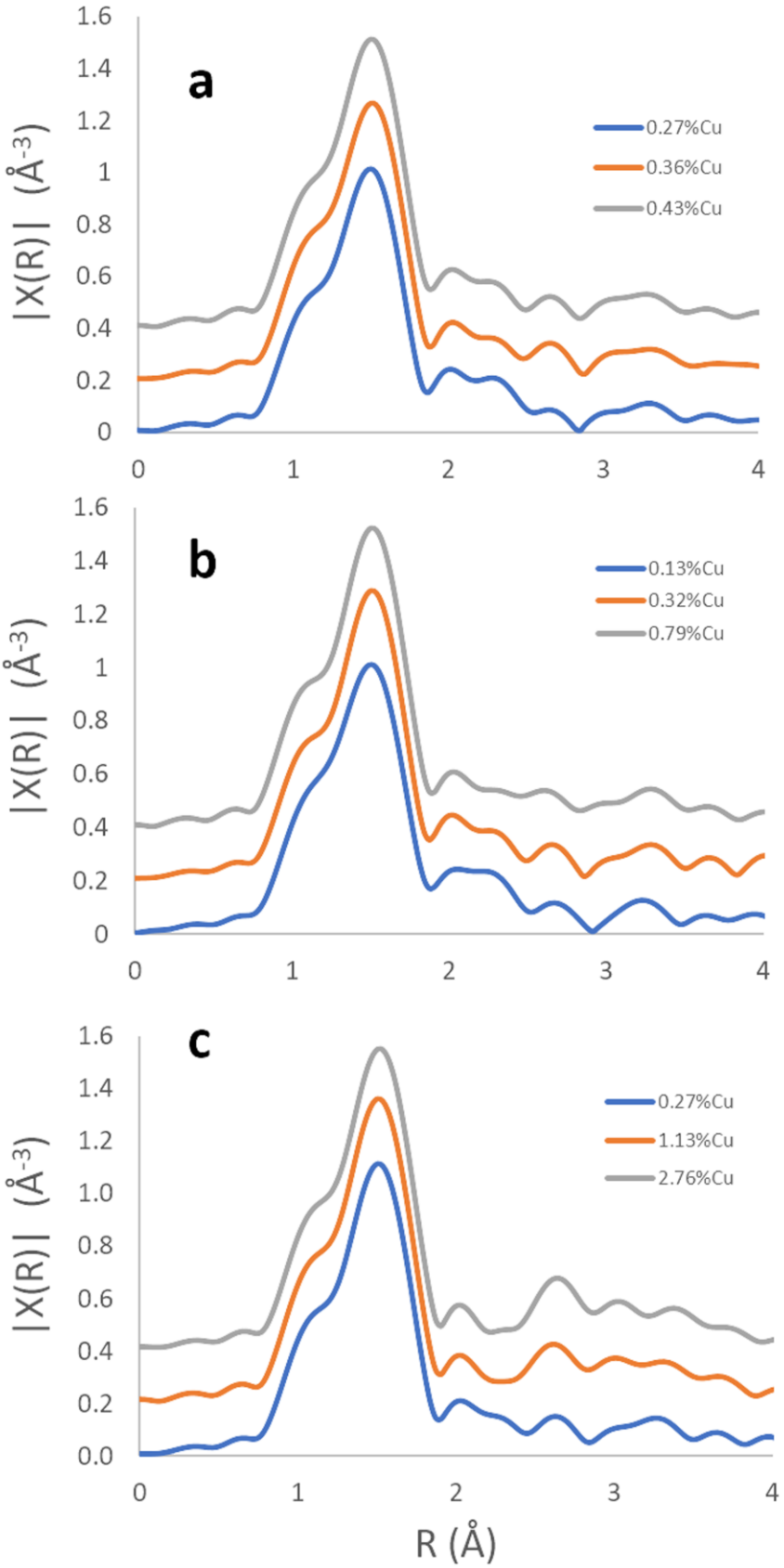

Fig. 3. FT of shifted experimental EXAFS data where a) represents the spectra at pH 4.5, b) pH 5.5 and c) pH 6.5 conditions each with different amount of adsorbed Cu.

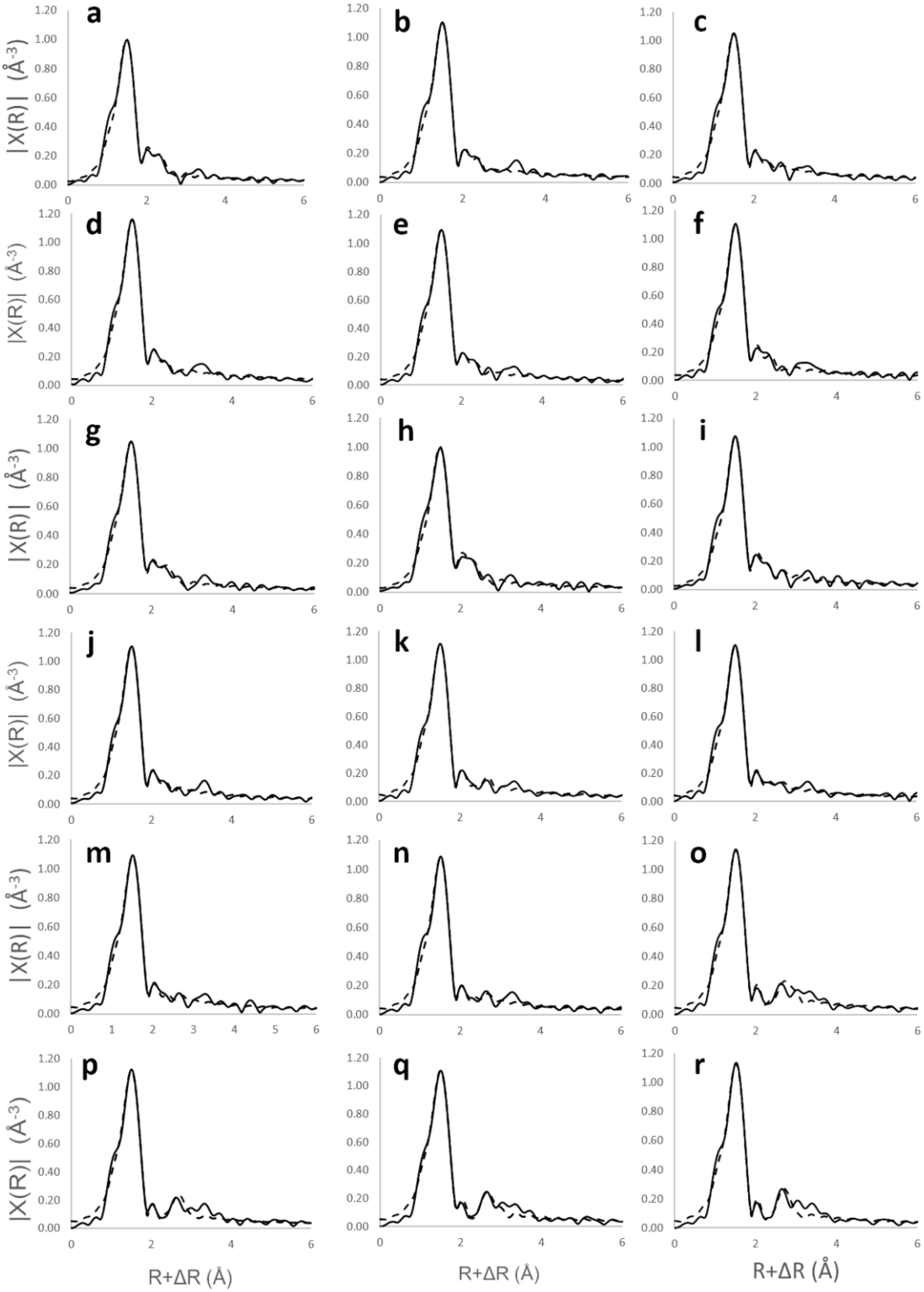

Fig. 4. Best fits of the FT EXAFS are given in dashed lines whereas the data is shown in solid lines, for the samples: a) pH 4.5-0.27%, b) pH 4.5-0.32%, c) pH 4.5-0.36%, d) pH 4.5-0.37%, e) pH 4.5-0.43%, f) pH 4.5-0.58%, g) pH 5.5 -0.12%, h) pH 5.5-0.13%, i) pH 5.5 -0.32%, j) pH 5.5-0.45%, k) pH 5.5-0.57%, l) pH 5.5 -0.79%, m) pH 6.5-0.27%, n) pH 6.5-0.52%, o) pH 6.5-1.13%, p) pH 6.5-1.31%, q) pH 6.5-2.76%, r) pH 6.5-2.76%. Fit parameters are given in Table 1.

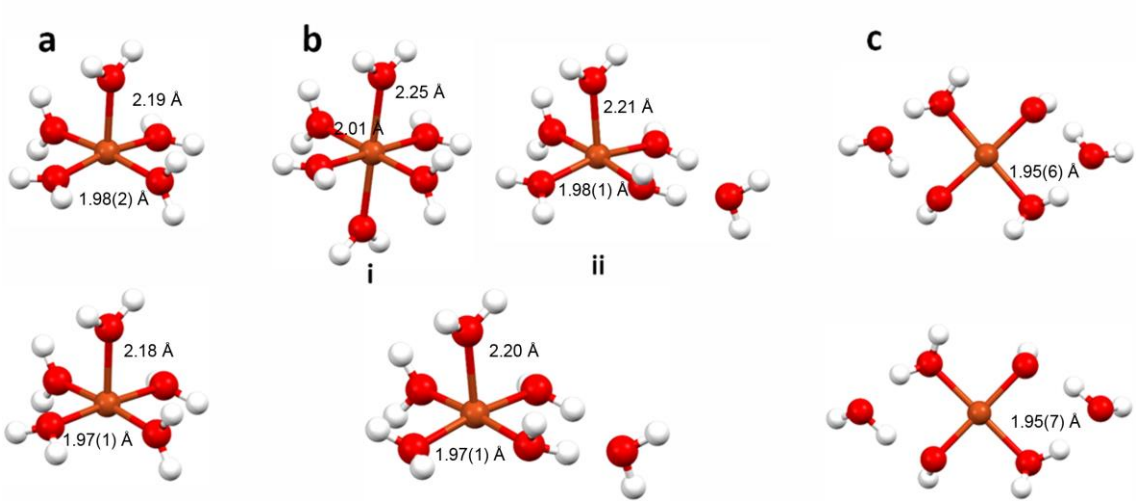

Fig. 5. Optimised geometries for the gas phase (top) and aqueous phase (bottom), for the configurations, a) $Cu(H_2O)_5$, b) $Cu(H_2O)_5 + H_2O$ and c) $Cu(OH)_2(H_2O)_4$ trans. Where i) represent results from calculations with the extra water molecule started at 2.3 Å and ii) at 2.8 and 3.3 Å. Final bond lengths with the respective uncertainty (when possible) is indicated. Synthesis of data also in Table S3 in SI.

LIST OF TABLES

Table 1. Results of EXAFS analyses.

		Cu-O_{eq}			Cu-O_{ax}						Cu-Cu			ΔE_0 [d]	R [e]
		N [a]	R [b] (Å)	σ [c] (Å)	N [a]	R [b] (Å)	σ [c] (Å)	N [a]	R [b] (Å)	σ [c] (Å)	N [a]	R [b] (Å)	σ [c] (Å)		
pH 4.5	0.27% Cu	2.8	1.94	0.005	*0.5*	2.68	0.008	1.0	3.19	0.011	- [f]	- [f]	- [f]	-4.1	0.008
	0.32% Cu	3.5	1.95	0.005	0.7	2.25	0.010	0.6	3.13	0.010	- [f]	- [f]	- [f]	-2.0	0.005
	0.36% Cu	3.7	1.96	0.006	0.8	2.25	0.008	0.6	3.04	0.011	- [f]	- [f]	- [f]	-1.8	0.010
	0.37% Cu	3.9	1.95	0.006	0.7	2.25		0.7	3.10	0.010	- [f]	- [f]	- [f]	-2.3	0.004
	0.43% Cu	3.6	1.95	0.006	*0.5*	2.25	0.010	0.6	3.10	0.010	- [f]	- [f]	- [f]	-2.8	0.007
	0.58% Cu	3.4	1.95	0.005	0.6	2.23	0.010	0.7	3.16	0.010	- [f]	- [f]	- [f]	-2.7	0.007
pH 5.5	0.12% Cu	3.5	1.95	0.006	*0.5*	2.26	0.010	1.0	3.24	0.010	- [f]	- [f]	- [f]	-3.3	0.006
	0.13% Cu	3.0	1.94	0.005	*0.5*	2.67	0.004	0.9	3.20	0.010	- [f]	- [f]	- [f]	-4.2	0.012
	0.32% Cu	2.8	1.94	0.004	0.6	2.67	0.003	0.6	3.00	0.010	- [f]	- [f]	- [f]	-3.0	0.009
	0.45% Cu	3.6	1.95	0.006	0.8	2.25	0.010	0.6	3.07	0.010	- [f]	- [f]	- [f]	-2.0	0.005
	0.57% Cu	3.8	1.96	0.006	0.7	2.25	0.006	0.7	3.00	0.003	- [f]	- [f]	- [f]	-1.9	0.004
	0.79% Cu	3.5	1.95	0.005	0.6	2.24	0.008	0.7	2.99	0.009	- [f]	- [f]	- [f]	-2.1	0.007
pH 6.5	0.27% Cu	3.5	1.95	0.005	0.6	2.24	0.010	0.7	3.01	0.010	- [f]	- [f]	- [f]	-2.5	0.007
	0.52% Cu	3.5	1.95	0.005	0.7	2.25	0.010	1.0	3.00	0.009	- [f]	- [f]	- [f]	-2.0	0.009
	1.13% Cu	3.6	1.95	0.005	0.8	2.24	0.010	1.1	2.95	0.006	1.4	3.13	0.015	-1.8	0.010
	1.31% Cu	3.7	1.95	0.005	0.7	2.27	0.010	1.0	2.95	0.008	1.0	3.07	0.014	-2.6	0.008
	2.76% Cu	3.7	1.95	0.006	0.7	2.25	0.010	0.7	2.95	0.001	1.3	3.10	0.015	-2.6	0.005
	2.76% Cu	3.5	1.95	0.005	0.9	2.25	0.011	1.0	2.97	0.007	1.4	3.09	0.015	-1.7	0.008

a - Coordination number; b - Refined interatomic distance; c - Debye-Waller factor; d - Energy shift; e - Figure of merit of the fit; f - Better fits where obtained without the inclusion of such parameters.
Note that values in italic are at the limit of their restraint.

6